

Tree Representations of Brain Structural Connectivity via Persistent Homology

Didong Li¹, Phuc Nguyen², Zhengwu Zhang³ and David B Dunson²

*Department of Biostatistics¹ and Department of Statistics and Operations Research³
University of North Carolina at Chapel Hill
Department of Statistical Science², Duke University*

Abstract

The brain structural connectome is generated by a collection of white matter fiber bundles constructed from diffusion weighted MRI (dMRI), acting as highways for neural activity. There has been abundant interest in studying how the structural connectome varies across individuals in relation to their traits, ranging from age and gender to neuropsychiatric outcomes. After applying tractography to dMRI to get white matter fiber bundles, a key question is how to represent the brain connectome to facilitate statistical analyses relating connectomes to traits. The current standard divides the brain into regions of interest (ROIs), and then relies on an *adjacency matrix* (AM) representation. Each cell in the AM is a measure of connectivity, e.g., number of fiber curves, between a pair of ROIs. Although the AM representation is intuitive, a disadvantage is the high-dimensionality due to the large number of cells in the matrix. This article proposes a simpler tree representation of the brain connectome, which is motivated by ideas in computational topology and takes topological and biological information on the cortical surface into consideration. We demonstrate that our tree representation preserves useful information and interpretability, while reducing dimensionality to improve statistical and computational efficiency. Applications to data from the Human Connectome Project (HCP) are considered and code is provided for reproducing our analyses.

Key Words: Adjacency matrix, brain connectome, persistent homology, structural connectivity, tree.

1 Introduction

The human brain structural connectome, defined as the white matter fiber tracts connecting different brain regions, plays a central role in understanding how brain structure impacts human function and behavior (Park and Friston, 2013). Recent advances in neuroimaging

methods have led to increasing collection of high quality functional and structural connectome data in humans. There are multiple large datasets available containing 1,000s of connectomes, including the Human Connectome Project (HCP) and the UK Biobank (Essen et al., 2012; Bycroft et al., 2018). We can now better relate variations in the connectomes between individuals to phenotypic traits (Wang et al., 2012; Hong et al., 2019; Roy et al., 2019). However, the large amount of data also creates the need for informative and efficient representations of the brain and its structural connectome (Galletta et al., 2017; Zhang et al., 2018; Pizarro et al., 2019; Sotiropoulos and Zalesky, 2019; Jeurissen et al., 2019). The main focus of this article is a novel and efficient representation of the processed connectome data as an alternative to the adjacency matrix (AM) as input to statistical analyses.

Diffusion magnetic resonance imaging (dMRI) uses diffusion-driven displacement of water molecules in the brain to map the organization and orientation of white fiber tracts on a microscopic scale (Bihan, 2003). Applying tractography to the dMRI data, we can construct a “tractogram” of 3D trajectories of white fiber tracts (Jeurissen et al., 2019). It is challenging to analyze the tractogram directly because 1) the number of fiber trajectories is extremely large; 2) the tractogram contains geometric structure; and 3) alignment of individual tracts between subjects remains difficult (Zhang et al., 2019). Because of these challenges, it is common to parcellate the brain into anatomical regions of interest (ROIs) (Desikan et al., 2006; Destrieux et al., 2010; Wang et al., 2010), and then extract fiber bundles connecting ROIs. We can then represent the brain structural connectome as a weighted network in a form of an AM, a p by p symmetric matrix, with i, j -th entry equal to the number of fiber curves connecting region i and region j , where p is the total number of regions in the parcellation.

Statistical analyses of structural connectomes are typically based on this AM representation, which characterizes the connectome on a fixed scale depending on the resolution of ROIs. However, research has shown that brain networks fundamentally organize as multi-scale and hierarchical entities (Bassett and Siebenhühner, 2013). Some research has attempted to analyze community structures in functional and structural brain networks across resolutions (Betzl and Bassett, 2017); however, these works are limited to community detection. Brain atlases have anatomically meaningful hierarchies but only one level can be captured by the AM representation. If the lowest level in the atlas hierarchy with the greatest number of ROIs is used, this creates a very high-dimensional representation of the brain. The number of pairs of ROIs often exceeds the number of connectomes in the dataset. This presents statistical and computational challenges, with analyses often having

low power and a lack of interpretability (Poldrack et al., 2017; Cremers et al., 2017).

For instance, to infer relationships between the connectome and a trait of interest, it is common to conduct hypothesis tests for association between each edge (connection strength between a pair of ROIs) and the trait (Fornito et al., 2016; Gou et al., 2018; Wang et al., 2019; Lee and Son, 2021). As the number of edges is very large, such tests will tend to produce a large number of type I errors without multiple testing adjustment. If a Bonferroni adjustment is used, then the power for detecting associations between particular edges and traits will be very low. A common alternative is to control for false discovery rate, for example via the Benjamini-Hochberg approach (Genovese et al., 2002). However, such corrections cannot solve the inevitable increase in testing errors that occur with more ROIs. An alternative is to take into account the network structure of the data in the statistical analysis; see, for example Leek and Storey (2008); Fornito et al. (2016); Alberton et al. (2020). Such approaches can potentially improve power to detect differences while controlling type I errors through appropriate borrowing of information across the edges or relaxation of the independence assumption, but statistical and computational problems arise as the number of ROIs increases. Finally, it is common to vectorize the lower-triangular portion of the brain AM and then apply regression or classification methods designed for high-dimensional features (e.g., by penalizing using the ridge or lasso penalties).

To make the problems more concrete, note that a symmetric $p \times p$ connectome AM has $\frac{(p-1)p}{2}$ pairs of brain ROIs. For the popular Desikan-Killiany parcellation (Desikan et al., 2006) with $p = 68$, $\frac{(p-1)p}{2} = 2278$. A number of other common atlases have many more than $p = 68$ brain regions, leading to a much larger number of edges. Even if one is relying on data from a large cohort, such as the UK Biobank, the sample size (number of subjects) is still much smaller than the connectivity features, leading to statistical efficiency problems without reducing the dimensionality greatly from $q = \frac{(p-1)p}{2}$. Dimensionality reduction methods, such as Principal Components Analysis (PCA), tensor decomposition, or non-negative matrix factorization, can be a remedy for studying relationships between the connectome and traits (Yourganov et al., 2014; Smith et al., 2015; Zhang et al., 2019; Patel et al., 2020). But, they may lack interpretability and fail to detect important relationships when the first few principal components are not biologically meaningful or predictive of traits.

In this paper, we propose a new representation of the brain connectome that is inspired by ideas in computational topology, a field focused on developing computational tools for investigating topological and geometric structure in complex data (Carlsson, 2009; Edels-

brunner and Harer, 2010). A common technique in computational topology is *persistent homology*, which investigates geometry/topology of the data by assessing how features of the data come and go at different scales of representation. Related ideas have been used successfully in studying brain vascular networks (Bendich et al., 2016), hippocampal spatial maps (Dabaghian et al., 2012), dynamical neuroimaging spatiotemporal representations (Geniesse et al., 2019), neural data decoding (Rybakken et al., 2019) and so on (Sizemore et al., 2019). We propose a fundamentally different framework, which incorporates an anatomically meaningful hierarchy of brain regions within a persistent homology approach to produce a new tree representation of the brain structural connectome. This representation reduces dimensionality substantially relative to the AM approach, leading to statistical and computational advantages, while enhancing interpretability. After showing our construction and providing mathematical and biological justification, we contrast the new representation with AM representations in analyses of data from the Human Connectome Project (HCP).

2 Method

2.1 Tree construction

There is a rich literature defining a wide variety of parcellations of the brain into regions of interest (ROIs) that are motivated by a combination of biological and statistical justifications (Desikan et al., 2006; Destrieux et al., 2010; Klein and Tourville, 2012). The ROIs should ideally be chosen based on biological function and to avoid inappropriately merging biologically and structurally distinct regions of the brain. Also, it is important to not sub-divide the brain into regions that are so small that (a) it may be difficult to align the data for different subjects and (b) the number of ROIs is so large that the statistical and computational problems mentioned in the introduction are exacerbated. Based on such considerations, the Desikan-Killiany (DK) atlas is particularly popular, breaking the brain into $p = 68$ ROIs (Desikan et al., 2006).

A parcellation such as DK is typically used to construct an AM representation of the structural connectome at a single level of resolution. However, we instead propose to introduce a multi-resolution tree in which we start with the entire cortical surface of the brain as the root node, and then divide into the right and left hemisphere to produce two children of the root node. We further sub-divide the two hemispheres into large sub-regions, then divide these sub-regions into smaller regions. We continue this sub-division until obtaining

the regions of DK (or another target atlas) as the leaf nodes in the tree. In doing this, we note that there is substantial flexibility in defining the tree structure; we need not choose a binary tree and can choose the regions at each level of the tree based on biological function considerations to the extent possible. Finally, we summarize the connectivity information at different resolutions in the weights of the tree nodes.

In this article, we focus primarily on the following tree construction based on the DK atlas for illustration, while hoping that this work motivates additional work using careful statistical and biological thinking to choose the regions at each layer of the tree. The DK parcellation is informed by standard neuroanatomical conventions, previous works on brain parcellations, conversations with expert scientists in neuroscience, and anatomic information on local folds and grooves of the brain (Desikan et al., 2006). The DK protocol divides each hemisphere into 34 regions that can be organized hierarchically (Desikan et al., 2006). Specifically, each hemisphere has six regions: frontal lobe, parietal lobe, occipital lobe, cingulate cortex, temporal lobe, and insula. Most of these regions have multiple sub-regions, many of which are further sub-divided in the DK atlas. The full hierarchy can be found in the Appendix. We calculate the weight of each node as the sum of all connections between its immediate children. For instance, the weight at the root node will equal the sum of all the inter-hemisphere connections. The weight of the left hemisphere node will equal the sum of all connections among the left temporal lobe, frontal lobe, parietal lobe, occipital lobe, cingulate cortex, and insula. The weight of the left temporal lobe is the sum of all connections between regions within the temporal medial aspect and lateral aspect. We continue this calculation for all nodes that have children. The weights of a leaf node will be all connections within that region, or equivalently, the diagonal element at that region’s index on the AM representation.

To rephrase the tree construction in math notations, let $A = A_1^1$ be the whole brain, A_1^2 be the left hemisphere, A_2^2 be the right hemisphere, and A_i^l be the i -th region at level l , where $l = 1, \dots, L$ and $i = 1, \dots, N_l$ ($L = 4$, $N_L = 10$ for DK). Define the weight of region A_i^l , denoted by H_i^l , as $H_i^l :=$ number of fibers connecting any two children of A_i^l for all $l = 1, 2, \dots, L$ and $i = 1, \dots, N_l$. For example, for DK-based tree, H_1^2 is the number of fibers connecting children of left hemisphere, that is, fibers between temporal lobe, cingulate cortex, occipital lobe, parietal lobe, and frontal lobe. Similarly, H_1^3 is the number of fibers connecting children of temporal lobe, that is, fibers between medial aspect and lateral aspect.

Figure 1 provides an illustration of the DK-based tree structure and the connections summarized at each node. Often the connections within the leaf nodes are not estimated

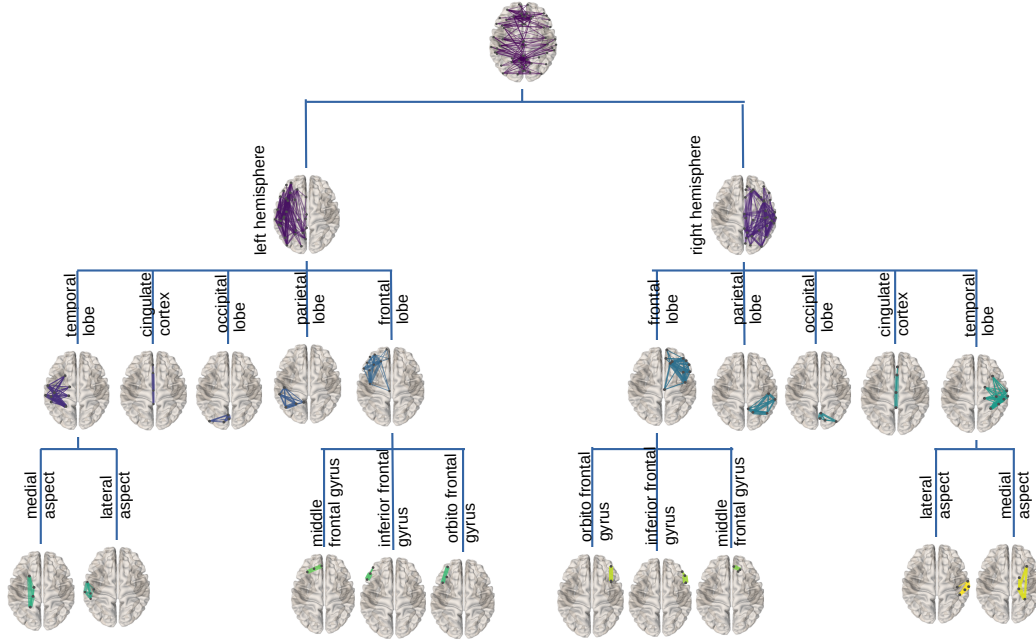


Figure 1: Visualization of the DK tree structure and connections summarized at each node on the brain image. Leaves have no internal connections and are omitted for readability.

in the AM representation (i.e., the diagonal elements of an AM are set to zero), thus, they have weights zero and are omitted from the figure. We also introduce a more compact visualization of the tree based on circle chord plots. Figure 2 shows the steps in our pipeline to construct a brain tree. The final output circle plot displays bundles of white matter tracts as overlapping chords scaled inversely proportional to the level of the tree they belong to and color-coded by the node they belong to.

2.2 A Persistent Homology Interpretation

Persistent homology is a method for computing topological features of a space at different resolutions. As quantitative features of noisy data, persistent homology is less sensitive to the choice of coordinate and metric and robust to noise (Carlsson, 2009). The key construction in persistent homology is the filtration, a multi-scale structure similar to the brain network. As a result, we can interpret the above defined H_k^l as corank of the persistent homology. As a rigorous definition of persistent homology is highly technical, we present a simple version

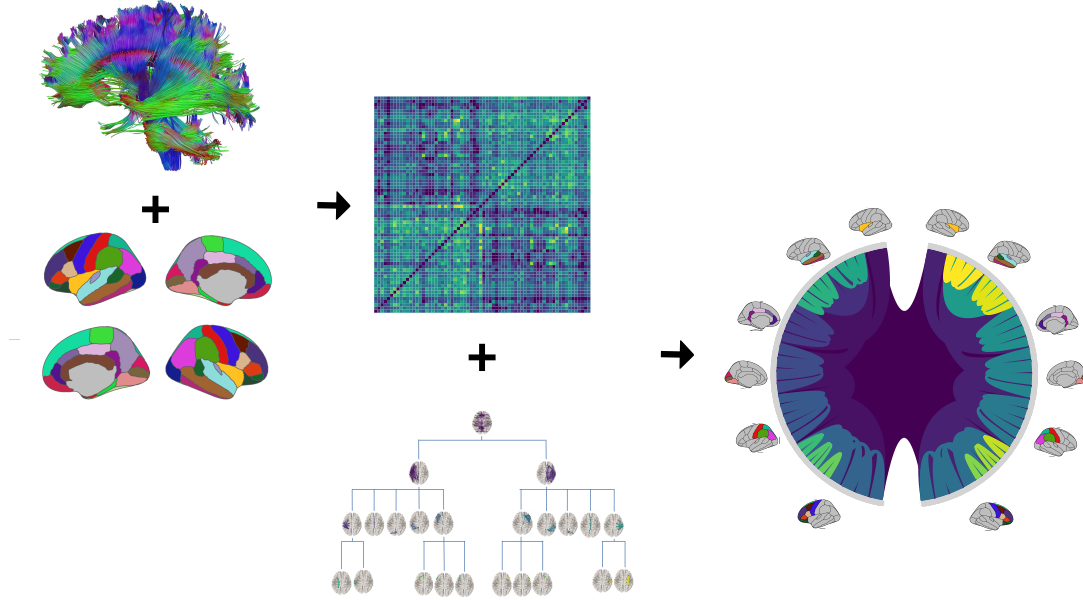


Figure 2: The tree construction pipeline: first, tractography and Desikan-Killiany (DK) protocol are used to estimate an adjacency matrix; then, the adjacency matrix and a hierarchy based on the DK protocol are combined to produce the tree representation. We introduce a compact circle chord plot that shows the tree representation of white matter fiber tracts connecting brain regions from the DK protocol. Connections are color-coded by the node they belong to, the same color codes as in Figure 1, and scaled inversely proportional to the level they belong to in the tree.

and leave the rigorous version and the proof to the Appendix. For relevant background in topology, see Munkres (2016); Hatcher (2002).

Theorem 1. H_k^l is the corank of the persistent homology.

Theorem 1 provides a topological interpretation of H_k^l , and partially explains why the tree $T = (A, H)$ is a powerful representation of the brain network.

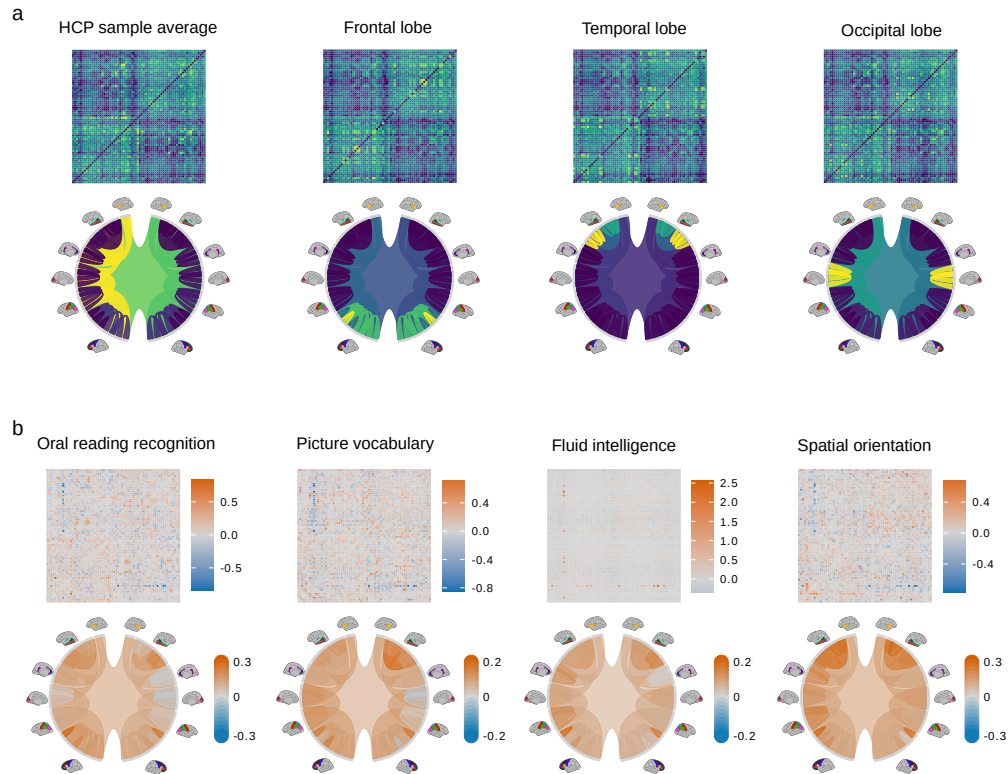


Figure 3: Examples of adjacency matrices and corresponding tree representations of brain connectomes. a) The sample average from the HCP data (left most) and its modifications so that different regions of the brain (i.e. the frontal lobe, temporal lobe, and occipital lobe) have denser connections. Because these modifications are unrealistic and only meant for better visualization of the differences between AM and tree representations, color scales are omitted. Values in the adjacency matrices are normalized for visual clarity. b) Percent difference in brain connections between the top and bottom ten percent of scores in four cognitive tasks.

3 Results

3.1 Data description

We investigate our tree representation’s ability to preserve information from the AM representation while improving interpretability in analyses relating brain structures to behavioral traits. We use neuroimaging data and scores on various behavioral assessments from the HCP (Glasser et al., 2013, 2016). The HCP collects high-quality diffusion MRI (dMRI) and structural MRI (sMRI) data, characterizing brain connectivity of 1200 healthy adults, and enables comparison between brain circuits, behavior and genetics at the individual subject level (Essen et al., 2012). We use data from the 2017 release accessed through ConnectomeDB. Details on data acquisition and preprocessing pipeline of dMRI and sMRI data in the HCP can be found in Essen et al. (2012); Glasser et al. (2013, 2016). To produce connectome data from raw dMRI/sMRI data, we use the reproducible probabilistic tractography algorithm in Girard et al. (2014) to construct tractography data for each subject, the DK atlas (Desikan et al., 2006) to define the brain parcellation, and the preprocessing pipeline in Zhang et al. (2018) to extract weighted matrices of connections. More details of these steps can be found in Zhang et al. (2019). In the extracted data matrices, each connection is described by a scalar number. The HCP data include scores for many behavioral traits related to cognition, motor skills, substance use, sensories, emotions, personalities, and many others. Details can be found at <https://wiki.humanconnectome.org/display/PublicData/HCP-YA+Data+Dictionary-+Updated+for+the+1200+Subject+Release>. The final data set consists of $n = 1065$ brain connectomes and 175 traits.

To study relationships between the AM and tree-based representations of the brain connectome, we use a simple two-step approach: first vectorizing the connectome data, and then applying a regression method. Since a connectome matrix is symmetric, we only vectorize the upper triangular part, resulting in a 2278-dimensional vector for each matrix. We also remove pairs of ROIs that show no variability in connectivity across subjects, reducing the vectorized matrices to 2202 dimensions. We construct the tree representations of the connectomes based on the construction described in Section 2.1. Self-edges are not recorded in the connectome matrices, so the leaves in the tree representation have zero weights. As a result, we remove the leaf nodes, leaving the vectorized trees to be 23-dimensional instead of 91-dimensional.

To apply regression algorithms, we first reduce the dimension of the adjacency matrix

to $K \ll 2202$ by selecting the top principal components (PCs). We observed that the regression MSEs of commonly used algorithms including linear regression, decision trees, support vector machines (SVM), boosting, Gaussian process (GP) regression, etc, did not decrease when we increased the number of PCs, and Zhang et al. (2019) also observed that the regression performance is robust for $K = 20 \sim 60$. As a result, we keep the first $K = 23$ PCs to match the dimension of the tree for a fair comparison. We refer to the data from the vectorized trees as D_{tree} and that from principal components of the vectorized matrices as D_{PCA} . Figure 3a compares the visualization of the average connectomes matrix to the average connectomes tree from the HCP data. Figure 3b shows the visualization of the tree representation as a more effective exploratory analysis tool since one can easily find regions of the brain with large percentage change between the top and bottom scores in four cognitive traits.

3.2 Canonical correlation analysis

Human brain connectivity has been shown to be capable of explaining significant variation in a variety of human traits. Specifically, data on functional and structural connectivity have been used to form latent variables that are positively correlated with desirable, positive traits (i.e., high scores on fluid intelligence or oral reading comprehension) while also being negatively correlated with undesirable traits (i.e., low sleep quality, frequent use of tobacco or cannabis) (Smith et al., 2015; Tian et al., 2020). In this first analysis, we compare how strongly latent variables inferred from the two representations are associated with the perceived desirability of traits. We choose to work with a subset of 45 traits that have been shown to strongly associate with brain connectome variations, including cognitive traits, tobacco/drug use, income, years of education, and negative and positive emotions (Zhang et al., 2019; Smith et al., 2015). Each cognitive trait is often measured by several metrics in an assessment. We only include a primary metric that has been adjusted for the subject’s age if applicable. We include only traits with continuous values to simplify the analyses. The full list of variables used can be found in the Appendix. We will use a statistical method called canonical correlation analysis (CCA), which finds linear combinations of the predictors that are most correlated with some other linear combinations of the outcomes. In our case, the predictors are principal components of the vectorized AM or features of the vectorized trees, and the outcomes are scores measured on 45 traits. Mathematically, let $X \in \mathbb{R}^{n \times p}$ be the feature matrix ($n = 1065, p = 23$), and $Y \in \mathbb{R}^{n \times q}$ be the outcome matrix ($q = 39$

with some traits being removed due to extensive missing values, see the next paragraph for more details). Additionally, let $\mathbf{a}_k \in \mathbb{R}^p$ and $\mathbf{b}_k \in \mathbb{R}^q$, $k = 1, \dots, \min(p, q)$ be pairs of linear transformation of the data. We refer to $(\mathbf{r}_k, \mathbf{s}_k) = (X\mathbf{a}_k, Y\mathbf{b}_k)$ as the feature and outcome canonical variates or the k^{th} pair of canonical variates. CCA aims to learn $\mathbf{a}_k, \mathbf{b}_k$ such that $(\mathbf{a}_k, \mathbf{b}_k) = \operatorname{argmax}_{\mathbf{a}_k, \mathbf{b}_k} \operatorname{corr}(\mathbf{r}_k, \mathbf{s}_k)$, so the linear transformations maximize the correlation between components of the canonical variates pair. Pairs of canonical variates are also constrained to be orthogonal, that is, $\mathbf{r}_k^T \mathbf{r}_h = 0$ and $\mathbf{s}_k^T \mathbf{s}_h = 0$ for $k \neq h$.

Since this analysis considers all traits simultaneously, we remove traits with extensive missing values (i.e., more than 10% of all observations) and are left with 39 traits. We then normalize D_{tree} , D_{PCA} and these 39 trait scores, and fill in missing values with the feature’s mean. We fit two CCAs using D_{tree} and D_{PCA} separately, and use the Wilks’s lambda test to check that the first canonical variate pair, which has the largest co-variation, is significant at the 5% level in each model. We hand-label the traits as desirable or not desirable based on previous research (Smith et al., 2015; Tian et al., 2020). Figure 4 plots the correlation of the trait scores with the first feature canonical variate and color-codes traits by desirability. Traits with smaller fonts have smaller contributions to the linear combination that makes up the first outcome canonical variate. It shows that desirable traits tend to be more highly negatively correlated with the first feature canonical variate compared to the undesirable traits, which tend to be weakly correlated. This is most clear with traits with strong signal such as fluid intelligence and spatial orientation. With the same number of features, the tree representation produces a canonical variate that can separate traits into groups of the same desirability slightly better than the principal components of the AM can.

3.3 Prediction

Additionally, we consider the performance of these representations in predictive tasks. We hypothesize that if the tree representation preserves important information from the AM representation, they will provide comparable performance in predicting trait scores. Since in section 3.2, cognitive traits generally have the largest correlations with the first feature canonical variate, we will examine cognitive traits in more details in this section. Specifically, we include all 45 cognitive traits in the HCP data, including different metrics of the same trait. We fit a baseline model that returns the sample mean and 19 popular machine learning models (including linear regression, decision tree, SVM, ensemble trees, GP regression, and their variants) to the D_{tree} and D_{PCA} data. To evaluate predictive performance, we consider



Figure 4: Correlations between behavioral traits and the first canonical variate extracted from 23 principal components of the AM compared to the 23 non-leaf nodes of the tree representation. The y-axis has been transformed so that traits do not overlap. The font size of each trait indicates the magnitude of the coefficients of a linear combination that defines the first canonical variate.

two scale-free metrics: 1) correlations between predictions and true outcomes and 2) the percentage of improvement in test MSE compared to the baseline predictor. We calculate these metrics using 5-fold cross validation repeated 10 times. Figure 5 shows the cross-validated

predictive performance for two representative regression algorithms: linear regression and GP regression. Linear regression represents a simple, interpretable, and widely used algorithm, while GP regression is a flexible algorithm that has the best overall performance among the 19 algorithms we studied. For each algorithm and each trait, the x -axis is the performance of the AM representation while the y -axis is that of the tree representation. Points above the diagonal line $y = x$ indicate better performance by the tree representation, while points below the line indicate better performance by the AM representation.

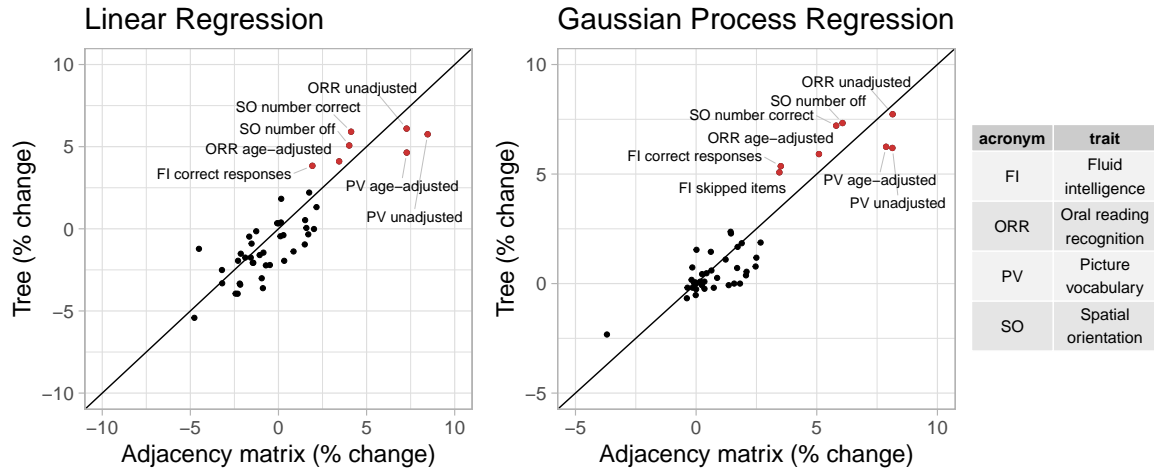


Figure 5: Percentage of change in MSE compared to baseline of linear regression and GP regression using tree and AM representation in predicting 45 cognitive traits

Overall, the performance of both representations seems similar. However, for most traits, even when considering the GP regression with best overall performance, the correlation is smaller than 0.2, and the improvement in test MSE is less than 3 percent. This suggests that the vectorized brain connectivity might not be relevant to predicting most of these traits. If we focus on traits with large correlations or improvement in MSE, the tree representation has better performance in terms of both correlation and improvement in MSE for five out of eight traits with correlations greater than 0.2. These traits include fluid intelligence, picture vocabulary, spatial orientation, and oral reading recognition, which also have the largest correlations with the canonical variate in section 3.2.

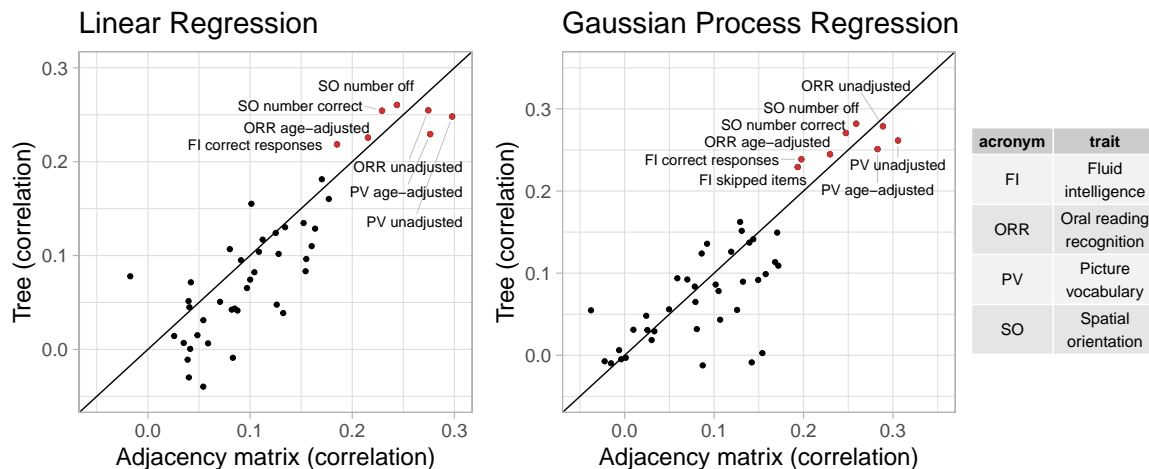


Figure 6: Correlation between predictions and observed outcomes of linear regression and GP regression using tree and AM representation in predicting 45 cognitive traits

3.4 Interpretability of regression

Finally, we compare interpretability of the two representations. Scientists are often interested in identifying structures in the connectomes that are associated with traits to answer questions such as which kind of connections might be damaged by routine use of drugs or which might be responsible for enhanced working memory. Therefore, we compare interpretability, in terms of biologically meaningful inference, of regression results using the two representations. We focus on spatial orientation (number correct), picture vocabulary (age-adjusted), fluid intelligence (correct responses), oral reading recognition (age-adjusted), and working memory (age-adjusted) because these traits show strong associations with the connectomes in the CCA and prediction tasks.

We fit a separate linear regression with Bayesian model selection on D_{tree} and D_{PCA} to infer associations between brain connectomes and the traits mentioned above. Bayesian model selection accounts for uncertainty in the model selection process by posterior probabilities for the different possible models. The regression coefficients are averaged across all models, weighted by estimated model posterior probabilities. For feature selection, we define important features as those with posterior inclusion probabilities of more than 0.75. For models using D_{tree} , we simply interpret posterior means and credible intervals of the estimated effects of important features directly. Figure 7 and Figure 8 (left column) show tree features whose colors are based on their estimated coefficients, and opacity are based

on their posterior inclusion probabilities.

For the models using D_{PCA} , after selecting important principal components, we can calculate a regression coefficient for each brain connection from the regression coefficients of these important principal components. Let X be an $n \times p$ matrix of vectorized brain connections whose columns have been standardized. Recall that PCA is based on the singular-value decomposition of the data matrix $X = UDV^T$, where $VV^T = I, U^TU = I$ and D is a diagonal matrix of p non-negative singular values, sorted in decreasing order. The j^{th} principal axis is the j^{th} eigenvector or the j^{th} column of V , and the j^{th} principal component is the j^{th} column of UD . With K PCs, we get a rank- K approximation of $X \approx U_K D_K V_K^T$ where M_K contains the first K columns of matrix M . Applying the approximation to the linear model $Y = X\beta + \epsilon \approx U_K D_K \theta + \epsilon$, we get $V_K^T \beta \approx \theta$, where θ is a K -vector of regression coefficients of the principal components. There are multiple generalized inverses $\hat{\beta} = V_K \theta + \mathbf{b}$ for \mathbf{b} such that $V_K^T \mathbf{b} = \mathbf{0}$. We will use $\mathbf{b} = \mathbf{0}$ to get the standard least-norm inverse $\hat{\beta} = V_K \theta$ as estimates of the regression coefficient for the original brain connections (West, 2003). We interpret the results based on 50 connections with the largest coefficient magnitude. Figure 7 and Figure 8 (right column) show these connections colored by their estimated coefficients.

The tree-based model finds no structure statistically significant (with posterior inclusion probability greater than 0.75) in predicting enhanced working memory. This is consistent with previous sections showing weak signals for associations between working memory and brain connectomes. The matrix-based model finds some cross-hemispheric connections between temporal lobes positively correlated with enhanced memory, which is supported by prior research (Eriksson et al., 2015). However, it also finds many right hemispheric connections negatively correlated with these scores, which contradicts some prior findings (Poldrack and Gabrieli, 1998). For oral reading recognition, the models find cross-hemispheric and left hemispheric connections important in both the tree and adjacency matrix representations. This is consistent with prior research that showed better reading ability associated with more cross-hemispheric connections between frontal lobes (Zhang et al., 2019) and with increased fractional anisotropy in some left hemispheric fiber tracts (Yeatman et al., 2012). The matrix-based model additionally finds many connections across all regions in the right hemisphere to be important, among which the insula, frontal opercular, and lateral temporal lobe have previously been found to correlate with this score (Kristanto et al., 2020). For fluid intelligence, the tree-based model finds connections within the left hemisphere and between hemispheres to be important. The matrix-based model finds within-hemisphere connections, especially those involving the frontal lobes, to be important. The fluid intel-

ligence score serves as proxy for “general intelligence” (Raven, 2000; Gershon et al., 2014), which relies on many sub-networks distributed across the brain (Dubois et al., 2018). For the vocabulary task, the tree-based model finds connections within the left hemisphere, while the matrix-based model finds connections within both hemispheres, to be important. Both results support existing findings that interpreting meanings of words activates many regions across the brain (Huth et al., 2016). Finally, in the spatial orientation task, the tree-based model finds cross-hemispheric connections to be important and positively correlated with better scores, while the matrix-based model does for connections between regions within each hemisphere (Figure 8 bottom). Both are somewhat similar to prior research that found decreased cross-hemispheric and right hemispheric connectivity to be associated with impaired spatial recognition of stroke patients (Ptak et al., 2020). Overall, we observe that the results from the tree representation are easier to interpret because of the inherent low-dimensional and biologically meaningful structure. The results from the AM representation tend to be noisier, and more likely to involve negative correlations between connectivity and better performance in cognitive tasks. Potentially, the representations may better encode different kinds of information that are both important.

4 Discussion

We propose a novel and efficient tree representation based on persistent homology for the brain network. Through analyses of the HCP data, we show that the tree representation preserves information from the AM representation that relates brain structures to traits while being much simpler to interpret. Simultaneously, it reduces the computational cost and complexity of the analysis because of its inherent lower dimension. We believe the advantages of the tree representation will be more evident on small brain imaging data sets.

Our new representation opens doors to new mathematical and statistical methods to analyze brain connectomes; in particular, taking into account the tree structure of the data. Topological data analysis (TDA) uses notions of shapes and connectivity to find structure in data, and persistent homology is one of the most well-known TDA methods (Wasserman, 2017). TDA has been used successfully in studying brain networks (Saggar et al., 2018; Gracia-Tabuenca et al., 2020), but we provide a fundamentally different approach. Our analyses of the connectome trees in this paper are simplistic. We treat tree nodes as independent and non-interacting. Future work should consider the tree structure to enforce dependence between the nodes, and hence, between their effects on behavioral traits.

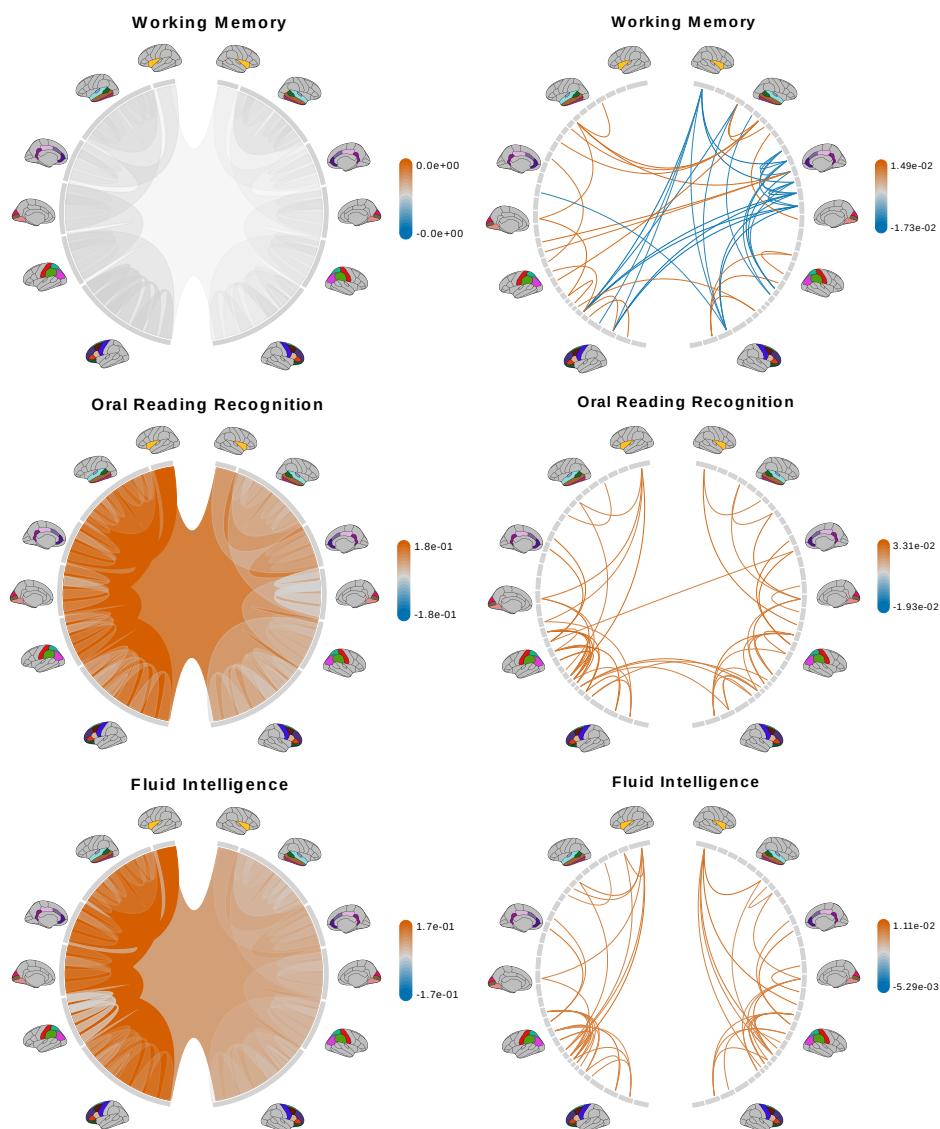


Figure 7: Brain connectome structures significantly associated with each trait inferred using the tree representation (left) and principal components of the AM representation (right). Colors represent the sign and magnitude of significant (i.e., posterior inclusion probability greater than 0.75) regression coefficients. For tree-based results, the opacity also represents the posterior inclusion probability.

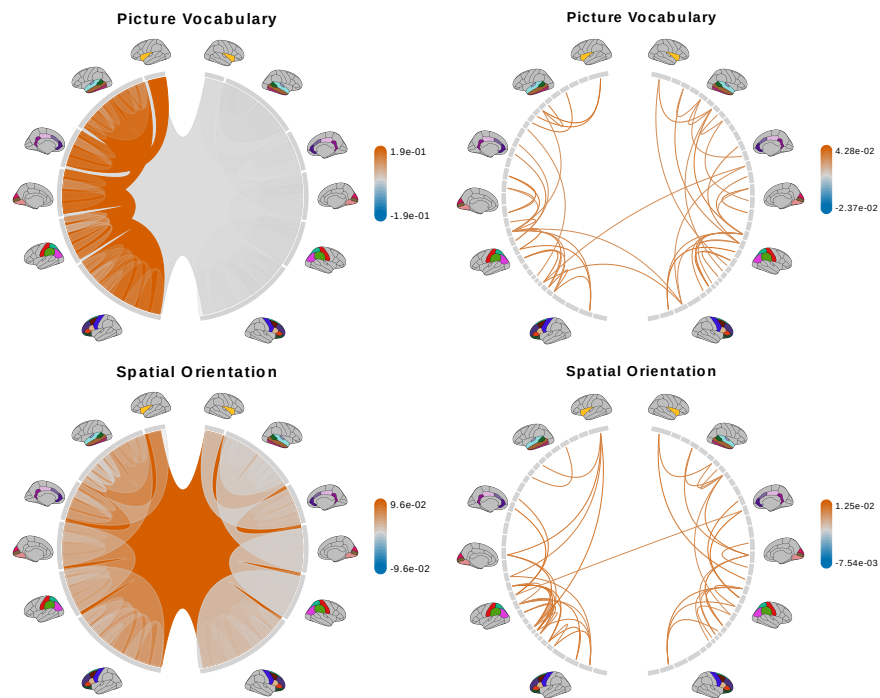


Figure 8: (Continue) Brain connectome structures significantly associated with each trait inferred using the tree representation (left) and principal components of the AM representation (right). Colors represent the sign and magnitude of significant (i.e., posterior inclusion probability greater than 0.75) regression coefficients. For tree-based results, the opacity also represents the posterior inclusion probability.

The tree structure may also be exploited to model interactions between connectome structures across different scales. For instance, Bayesian treed models are flexible, nonparametric methods that have found widespread and successful applications in many domains (Linero, 2017). Existing treed models might prove unwieldy to fit and interpret on AM-based brain networks but their modifications may fit the nature of our tree representation well.

5 Appendix

5.1 Hierarchy in one hemisphere based on the Desikan-Killiany protocol

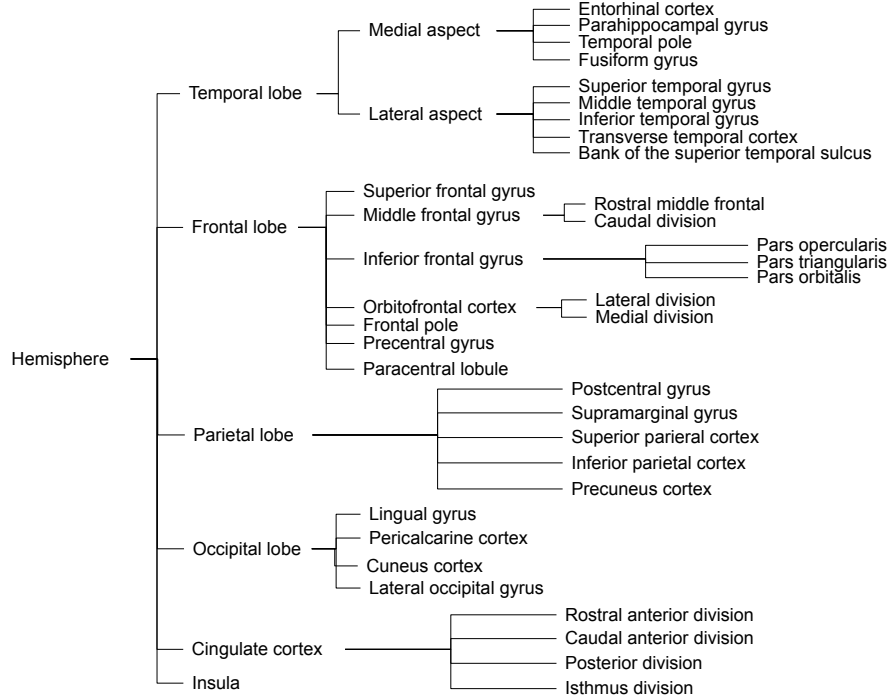


Figure 9: The full brain hierarchy based on the Desikan-Killiany protocol for one hemisphere.

5.2 Proof of theorem in Section 2

We first restate Theorem 1 in topological language. Let $x_j^l \in A_j^l$ be any location in brain region A_j^l and any fiber inside A_j^l is treated as a loop at x_j^l , denoted by $c_{j(1)}^l, \dots, c_{j(N_j^l)}^l$. So topologically speaking each region A_j^l consists of a point (0-cell) and N_j^l loops (1-cell).

Assume A_i^l and A_j^l are children of A_k^{l-1} , then we have a inclusion map from the children to the parent: $F_k^l : A_i^l \cup A_j^l \rightarrow A_k^{l-1}$, $F(x_j^l) = F(x_i^l) = x_k^{l-1}$, so F_k^l induces a homomorphism between chain groups: $F_k^l : C_p(A_i^l \cup A_j^l) \rightarrow C_p(A_k^{l-1})$, $p = 0, 1$. Observe that F maps all loops $c_{j(k)}^l$ and $c_{i(k)}^l$ to loops in A_k^{l-1} while any fiber (path) connecting A_i^l and A_j^l is also mapped to loops in A_k^{l-1} .

Theorem 1'. H_k^l is the corank of the persistent homology $F_{k*}^l \left(H_p(A_i^l \cup A_j^l) \right) \subset H_p(A_k^{l-1})$.

Before proving the theorem, we prove the following useful lemma:

Lemma 1. F defined above is a chain map so it induces a homomorphism between homology groups:

$$F_{k*}^l : H_p(A_i^l \cup A_j^l) \rightarrow H_p(A_k^{l-1}), p = 0, 1.$$

Proof. Since the chain group is nontrivial for $p = 0$ and $p = 1$ only, it suffices to check $\partial \circ F_k^l(c) = F_k^l \circ \partial(c)$ for any $c \in C_1(A_i^l \cup A_j^l)$.

If c is a loop, then $F_k^l(c)$ is also a loop by the construction of F_k^l , so we have $\partial \circ F(c) = x_k^{l-1} - x_k^{l-1} = 0$, $F_k^l \circ \partial(c) = F_k^l(0) = 0$.

If c is not a loop, we assume c starts from x_j^l ends at x_i^l , so $F_k^l(c)$ is still a loop, so we have $\partial \circ F_k^l(c) = x_k^{l-1} - x_k^{l-1} = 0$. Since $F_k^l \circ \partial(c) = F_k^l(x_i^l - x_j^l) = x_k^{l-1} - x_k^{l-1} = 0$, we conclude that $\partial \circ F_k^l = F_k^l \circ \partial$. \square

Now we can prove Theorem 1':

Proof of Theorem 1'. From the proof of Lemma 1, $\text{rank}(H_p(A_k^{l-1}))$ is the sum of the number of fibers in A_i^l and A_j^l as well as the number of fibers connecting A_i^l and A_j^l . Since all homologous classes in $H_p(A_i^l \cup A_j^l)$ are mapped to nontrivial homologous classes in $H_p(A_k^{l-1})$, $\text{rank} \left(F_{k*}^l \left(H_p(A_i^l \cup A_j^l) \right) \right) = \text{rank} \left(H_p(A_i^l \cup A_j^l) \right)$, which is equal to the number of fibers in fibers in A_i^l and A_j^l . As a result,

$$\text{corank} \left(F_{k*}^l \left(H_p(A_i^l \cup A_j^l) \right) \right) = \text{rank}(H_p(A_k^{l-1})) - \text{rank} \left(F_{k*}^l \left(H_p(A_i^l \cup A_j^l) \right) \right) = H_k^l.$$

\square

5.3 Table of 45 traits used in section 3.2 analysis

Table 1 lists the different traits used in our analyses grouped into categories; we provide the names used in the HCP data files along with a link to look up a detailed definition of each

of these traits.

Trait category	HCP column names
Cognition	PMAT24_A_CR, ReadEng_AgeAdj, PicVocab_AgeAdj, IWRD_TOT, ProcSpeed_AgeAdj, DDisc_AUC_200, DDisc_AUC_40K, VSPLIT_TC, SCPT_TPRT, ListSort_AgeAdj, PicSeq_AgeAdj, SSAGA_Educ, SSAGA_Income, CardSort_AgeAdj, Flanker_AgeAdj
Emotion	ER40_CRT, AngAffect_Unadj, AngHostil_Unadj, AngAggr_Unadj, FearAffect_Unadj, FearSomat_Unadj, Sadness_Unadj, PercStress_Unadj, SelfEff_Unadj, LifeSatisf_Unadj, MeanPurp_Unadj, PosAffect_Unadj
Tobacco use	SSAGA_TB_Age_1st_Cig, SSAGA_TB_DSM_Difficulty_Quitting, SSAGA_TB_Max_Cigs, SSAGA_TB_Reg_CPD, SSAGA_TB_Yrs_Smoked, Times_Used_Any_Tobacco_Today, Avg_Weekend_Any_Tobacco_7days, Total_Cigars_7days, Avg_Weekend_Cigars_7days, Num_Days_Used_Any_Tobacco_7days
Drug use	SSAGA_Times_Used_Illicits, SSAGA_Times_Used_Cocaine, SSAGA_Times_Used_Hallucinogens, SSAGA_Times_Used_Opiates, SSAGA_Times_Used_Sedatives, SSAGA_Times_Used_Stimulants, SSAGA_Mj_Age_1st_Use, SSAGA_Mj_Times_Used

Table 1: Column names from the HCP data file of traits used in our analysis, grouped by categories defined by their meanings. Since there are many metrics for the same trait, we provide the column names so that their exact definitions can be looked up at <https://wiki.humanconnectome.org/display/PublicData/HCP-YA+Data+Dictionary-+Updated+for+the+1200+Subject+Release>.

Acknowledgement

This work was partially supported by NIH grant R01-MH118927 by the United States National Institute of Mental Health and P30ES010126 by National Institute of Environmental Health Sciences.

References

- Alberston, B. A., Nichols, T. E., Gamba, H. R., and Winkler, A. M. (2020). Multiple testing correction over contrasts for brain imaging. *NeuroImage*, 216:116760.
- Bassett, D. S. and Siebenhühner, F. (2013). Multiscale network organization in the human brain. In Pesenson, M. Z., editor, *Multiscale Analysis and Nonlinear Dynamics*, chapter 7.
- Bendich, P., Marron, J. S., Miller, E., Pieloch, A., and Skwerer, S. (2016). Persistent homology analysis of brain artery trees. *The Annals of Applied Statistics*, 10(1):198.
- Betzal, R. F. and Bassett, D. S. (2017). Multi-scale brain networks. *NeuroImage*, 160:73–83.
- Bihan, D. L. (2003). Looking into the functional architecture of the brain with diffusion mri. *Nature Reviews Neuroscience*, 4:469–480.
- Bycroft, C., Freeman, C., Petkova, D., Band, G., Elliott, L. T., Sharp, K., Motyer, A., Vukcevic, D., Delaneau, O., Jared O’Connell, A. C., Welsh, S., Young, A., Effingham, M., McVean, G., Leslie, S., Allen, N., Donnelly, P., and Marchini, J. (2018). The UK Biobank resource with deep phenotyping and genomic data. *Nature*, 562:203–209.
- Carlsson, G. (2009). Topology and data. *Bulletin of the American Mathematical Society*, 46(2):255–308.
- Cremers, H. R., Wager, T. D., and Yarkoni, T. (2017). The relation between statistical power and inference in fMRI. *PloS one*, 12(11):e0184923.
- Dabaghian, Y., Mémoli, F., Frank, L., and Carlsson, G. (2012). *A topological paradigm for hippocampal spatial map formation using persistent homology*. Public Library of Science San Francisco, USA.
- Desikan, R. S., Ségonne, F., Fischl, B., Quinn, B. T., Dickerson, B. C., Blacker, D., Buckner, R. L., Dale, A. M., Maguire, R. P., Hyman, B. T., et al. (2006). An automated labeling system for subdividing the human cerebral cortex on MRI scans into gyral based regions of interest. *NeuroImage*, 31(3):968–980.
- Destrieux, C., Fischl, B., Dale, A., and Halgren, E. (2010). Automatic parcellation of human cortical gyri and sulci using standard anatomical nomenclature. *NeuroImage*, 53(1):1–15.

- Dubois, J., Galdi, P., Paul, L. K., and Adolphs, R. (2018). A distributed brain network predicts general intelligence from resting-state human neuroimaging data. *Philosophical Transactions of the Royal Society B: Biological Sciences*, 373(1756):20170284.
- Edelsbrunner, H. and Harer, J. (2010). *Computational topology: an introduction*. American Mathematical Soc.
- Eriksson, J., Vogel, E., Lansner, A., Bergström, F., and Nyberg, L. (2015). Neurocognitive architecture of working memory. *Neuron*, 88(1):33–46.
- Essen, D. C. V., Ugurbil, K., Auerbach, E., Barch, D., Behrens, T. E. J., Bucholz, R., Chang, A., Chen, L., Corbetta, M., Curtiss, S. W., Penna, S. D., Feinberg, D., Glasser, M. F., Harel, N., Heath, A. C., Larson-Prior, L., Marcus, D., Michalareas, G., Moeller, S., Oostenveld, R., Petersen, S. E., Prior, F., Schlaggar, B. L., Smith, S. M., Snyder, A. Z., Xu, J., Yacoub, E., and Consortium, W.-M. H. (2012). The human connectome project: a data acquisition perspective. *NeuroImage*, 62(4):2222–31.
- Fornito, A., Zalesky, A., and Bullmore, E. T. (2016). Chapter 11 - statistical connectomics. In *Fundamentals of Brain Network Analysis*, pages 383–419. Academic Press, San Diego.
- Galletta, A., Celesti, A., Tusa, F., Fazio, M., Bramanti, P., and Villari, M. (2017). Big mri data dissemination and retrieval in a multi-cloud hospital storage system. *Proceedings of the 2017 International Conference on Digital Health*, pages 162–166.
- Geniesse, C., Sporns, O., Petri, G., and Saggat, M. (2019). Generating dynamical neuroimaging spatiotemporal representations (dyneur) using topological data analysis. *Network Neuroscience*, 3(3):763–778.
- Genovese, C. R., Lazar, N. A., and Nichols, T. (2002). Thresholding of statistical maps in functional neuroimaging using the false discovery rate. *NeuroImage*, 15(4):870–8.
- Gershon, R. C., Cook, K. F., Mungas, D., Manly, J. J., Slotkin, J., Beaumont, J. L., , and Weintraub, S. (2014). Language measures of the NIH toolbox cognition battery. *J Int Neuropsychol Soc*, 20(6):642–651.
- Girard, G., Whittingstall, K., Deriche, R., and Descoteaux, M. (2014). Towards quantitative connectivity analysis: reducing tractography biases. *NeuroImage*, 98:266–278.

- Glasser, M. F., Smith, S. M., Marcus, D. S., Andersson, J. L. R., Auerbach, E. J., Behrens, T. E. J., Coalson, T. S., Harms, M. P., Jenkinson, M., Moeller, S., Robinson, E. C., Sotiropoulos, S. N., Xu, J., Yacoub, E., Ugurbil, K., and Essen, D. C. V. (2016). The Human Connectome Project’s neuroimaging approach. *Nature Neuroscience*, 19:1175–1187.
- Glasser, M. F., Sotiropoulos, S. N., Wilson, J. A., Coalson, T. S., Fischl, B., Andersson, J. L., Xu, J., Jbabdi, S., Webster, M., Polimeni, J. R., Essen, D. C. V., Jenkinson, M., and Consortium, W.-M. H. (2013). The minimal preprocessing pipelines for the human connectome project. *NeuroImage*, 80:105–24.
- Gou, L., Zhang, W., Li, C., Shi, X., Zhou, Z., Zhong, W., Chen, T., Wu, X., Yang, C., and Guo, D. (2018). Structural brain network alteration and its correlation with structural impairments in patients with depression in de novo and drug-naïve Parkinson’s disease. *Frontiers in Neurology*, 9:608.
- Gracia-Tabuenca, Z., Díaz-Patiño, J. C., Arelio, I., and Alcauter, S. (2020). Topological data analysis reveals robust alterations in the whole-brain and frontal lobe functional connectomes in attention-deficit/hyperactivity disorder. *eNeuro*, 7(3).
- Hatcher, A. (2002). *Algebraic topology*. Cambridge University Press.
- Hong, S.-J., Vos de Wael, R., Bethlehem, R. A., Larivière, S., Paquola, C., Valk, S. L., Milham, M. P., Di Martino, A., Margulies, D. S., Smallwood, J., et al. (2019). Atypical functional connectome hierarchy in autism. *Nature communications*, 10(1):1–13.
- Huth, A. G., De Heer, W. A., Griffiths, T. L., Theunissen, F. E., and Gallant, J. L. (2016). Natural speech reveals the semantic maps that tile human cerebral cortex. *Nature*, 532(7600):453–458.
- Jeurissen, B., Descoteaux, M., Mori, S., and Leemans, A. (2019). Diffusion MRI fiber tractography of the brain. *NMR in Biomedicine*, 32.
- Klein, A. and Tourville, J. (2012). 101 labeled brain images and a consistent human cortical labeling protocol. *Frontiers in Neuroscience*, 6:171.
- Kristanto, D., Liu, M., Liu, X., Sommer, W., and Zhou, C. (2020). Predicting reading ability from brain anatomy and function: From areas to connections. *NeuroImage*, 218:116966.

- Lee, D. and Son, T. (2021). Structural connectivity differs between males and females in the brain object manipulation network. *PLoS ONE*, 16(6):e0253273.
- Leek, J. T. and Storey, J. D. (2008). A general framework for multiple testing dependence. *Proceedings of the National Academy of Sciences*, 105(48):18718–18723.
- Linero, A. (2017). A review of tree-based Bayesian methods. *CSAM*, 24:543–559.
- Munkres, J. R. (2016). *Topology*. Pearson India Education Services Pvt. Ltd.
- Park, H.-J. and Friston, K. (2013). Structural and functional brain networks: from connections to cognition. *Science*, 342(6158):1238411.
- Patel, R., Steele, C. J., Chen, A. G., Patel, S., Devenyi, G. A., Germann, J., Tardif, C. L., and Chakravarty, M. M. (2020). Investigating microstructural variation in the human hippocampus using non-negative matrix factorization. *NeuroImage*, 207:116348.
- Pizarro, R., Assemlal, H.-E., Nigris, D. D., Elliott, C., Antel, S., Arnold, D., and Shmuel, A. (2019). Algorithms to automatically identify the brain MRI contrast: implications for managing large databases. *Neuroinformatics*, 17:115–130.
- Poldrack, R. A., Baker, C. I., Durnez, J., Gorgolewski, K. J., Matthews, P. M., Munafò, M. R., Nichols, T. E., Poline, J.-B., Vul, E., and Yarkoni, T. (2017). Scanning the horizon: towards transparent and reproducible neuroimaging research. *Nature Reviews Neuroscience*, 18(2):115–126.
- Poldrack, R. A. and Gabrieli, J. D. (1998). Memory and the brain: what’s right and what’s left? *Cell*, 93(7):1091–1093.
- Ptak, R., Bourgeois, A., Cavelti, S., Doganci, N., Schnider, A., and Iannotti, G. R. (2020). Discrete patterns of cross-hemispheric functional connectivity underlie impairments of spatial cognition after stroke. *Journal of Neuroscience*, 40(34):6638–6648.
- Raven, J. (2000). The Raven’s progressive matrices: Change and stability over culture and time. *Cognitive Psychology*, 41:1–48.
- Roy, H. A., Griffiths, D. J., Aziz, T. Z., Green, A. L., and Menke, R. A. L. (2019). Investigation of urinary storage symptoms in Parkinson’s disease utilizing structural mri techniques. *Neurourology and Urodynamics*, 38:1168–1175.

- Rybakken, E., Baas, N., and Dunn, B. (2019). Decoding of neural data using cohomological feature extraction. *Neural computation*, 31(1):68–93.
- Saggar, M., Sporns, O., Gonzalez-Castillo, J., Bandettini, P. A., Carlsson, G., Glover, G., and Reiss, A. L. (2018). Towards a new approach to reveal dynamical organization of the brain using topological data analysis. *Nature Communications*, 9(1399).
- Sizemore, A. E., Phillips-Cremins, J. E., Ghrist, R., and Bassett, D. S. (2019). The importance of the whole: topological data analysis for the network neuroscientist. *Network Neuroscience*, 3(3):656–673.
- Smith, S., Nichols, T., Vidaurre, D., Winkler, A., Behrens, T., Glasser, M., Ugurbil, K., Barch, D., Essen, D. V., and Miller, K. (2015). A positive-negative mode of population covariation links brain connectivity, demographics and behavior. *Nature Neuroscience*, 18:1565–1567.
- Sotiropoulos, S. N. and Zalesky, A. (2019). *NMR in Biomedicine*, 32.
- Tian, Y., Margulies, D. S., Breakspear, M., and Zalesky, A. (2020). Topographic organization of the human subcortex unveiled with functional connectivity gradients. *Nature Neuroscience*, 23:1421–1432.
- Wang, J., Zuo, X., Dai, Z., Xia, M., Zhao, Z., Zhao, X., Jia, J., Han, Y., and He, Y. (2012). Disrupted functional brain connectome in individuals at risk for Alzheimer’s disease. *Biological Psychiatry*, 73(5):471–481.
- Wang, J., Zuo, X., and He, Y. (2010). Graph-based network analysis of resting-state functional MRI. *Frontiers in Systems Neuroscience*, 4:16.
- Wang, L., Zhang, Z., and Dunson, D. (2019). Symmetric bilinear regression for signal subgraph estimation. *IEEE Transactions on Signal Processing*, 67(7):1929–1940.
- Wasserman, L. (2017). Topological data analysis. *Annual Review of Statistics and Its Application*, 5:501–532.
- West, M. (2003). Bayesian factor regression models in the “large p, small n” paradigm. In *Bayesian Statistics*, pages 723–732. Oxford University Press.

- Yeatman, J. D., Dougherty, R. F., Ben-Shachar, M., and Wandell, B. A. (2012). Development of white matter and reading skills. *Proceedings of the National Academy of Sciences*, 109(44):E3045–E3053.
- Yourganov, G., Schmah, T., Churchill, N. W., Berman, M. G., Grady, C. L., and Strother, S. C. (2014). Pattern classification of fMRI data: applications for analysis of spatially distributed cortical networks. *NeuroImage*, 96:117–32.
- Zhang, Z., Allen, G. I., Zhu, H., and Dunson, D. (2019). Tensor network factorizations: relationships between brain structural connectomes and traits. *NeuroImage*, 197:330–343.
- Zhang, Z., Descoteaux, M., Zhang, J., Girard, G., Chamberland, M., Dunson, D., Srivastava, A., and Zhu, H. (2018). Mapping population-based structural connectomes. *NeuroImage*, 172:130–145.